OXFORD SERIES ON ADVANCED MANUFACTURING

Series Editors

J. R. Crookall
Milton C. Shaw
Nam P. Suh

Series Titles

John Benbow and John Bridgewater, *Paste Flow and Extrusion*
John L. Burbidge, *Period Batch Control*
John L. Burbidge, *Production Flow Analysis for Planning Group Technology*
Shiro Kobayashi, S. Oh, and T. Altan, *Metal Forming and the Finite-Element Method*
Milton C. Shaw, *Metal Cutting Principles, 2nd edition*
Milton C. Shaw, *Principles of Abrasive Processing*
Nam P. Suh, *The Principles of Design*
Daniel E. Whitney, *Mechanical Assemblies: Their Design, Manufacture, and Role in Product Development*

METAL CUTTING PRINCIPLES

Second Edition

Milton C. Shaw
Professor Emeritus of Engineering
Arizona State University

New York Oxford
OXFORD UNIVERSITY PRESS
2005

Oxford University Press

Oxford New York
Auckland Bangkok Buenos Aires Cape Town Chennai
Dar es Salaam Delhi Hong Kong Istanbul Karachi Kolkata
Kuala Lumpur Madrid Melbourne Mexico City Mumbai Nairobi
São Paulo Shanghai Taipei Tokyo Toronto

Published by Oxford University Press, Inc.
198 Madison Avenue, New York, New York 10016
www.oup.com

Oxford is a registered trademark of Oxford University Press

Library of Congress Cataloging-in-Publication Data
Shaw, Milton Clayton, 1915–
Metal cutting principles / Milton C. Shaw. — 2nd ed.
p. cm. —- (Oxford series on advanced manufacturing; 5)
Includes bibliographical references and index.
ISBN 0-19-514206-3 (cloth)
1. Metal-cutting. I. Title. II. Series.

TJ1185.S498 2004
671.5′3—dc22

2003064974

Printing number: 9 8 7 6 5 4 3 2 1

Printed in the United States of America
on acid-free paper

To my wife
Mary Jane

10 FRICTION

Friction which is the resisting force one surface experiences when it slides over another is always oppositely directed to the relative velocity vector for the two surfaces. The entire field of friction may be divided into two general regimes—lightly loaded sliders and heavily loaded sliders. Each of these will be briefly discussed followed by a consideration of the special friction conditions that pertain in metal cutting. What constitutes a lightly loaded slider will be defined in a later section. Tribology is the term used to cover the performance of surfaces relative to lubrication, friction, and wear. The complete tribological characteristics of lightly loaded sliding surfaces is treated in detail in the two-volume classical work by Bowden and Tabor (1950, 1964). Suh and Sin (1981) and Suh (1986) have discussed the relation between friction and wear.

LIGHTLY LOADED SLIDERS

Types of Sliding Contact

There are five types of sliding contact:

1. Fluid film lubrication. This is the ideal type of lubrication in which there is no metal-to-metal contact. The load is supported by a pressurized fluid film. Viscosity is the physical property of the system of major interest, and the principles of fluid mechanics enable the load capacity and friction characteristics of surfaces that are so lubricated to be computed. Well-designed journal and slider bearings are of this type.
2. Elastohydrodynamic lubrication. This is the type of lubrication in which the localized stresses in the bearing surfaces are sufficiently high to cause a significant change in surface geometry and the fluid pressures are sufficiently high to alter the effective viscosity of the fluid. The lubrication of gear teeth, cam surfaces, and rolling contact bearings is of this type. This is a special version of hydrodynamic lubrication.
3. Boundary lubrication. Here the film is not complete and the surfaces come together close enough so that the resulting frictional resistance is not entirely due to viscous drag. The surface finish and the physical and chemical properties of the surfaces and lubricant are of major interest. Effective boundary lubricants are usually additives consisting of long-chain polar molecules that are physically adsorbed on the high points of mating surfaces and tend to prevent metal-to-metal contact.

4. Extreme boundary lubrication. This is the type of lubrication that obtains under the most severe sliding conditions (highly loaded bearing surfaces operating at relatively low speed). The additive in this case reacts chemically with one of the bearing metals to form a low-shear-strength solid layer that prevents metal-to-metal contact, welding, and metal transfer (wear). The solid films that are formed are usually inorganic, have a high melting point, and hence are suitable for use at elevated temperatures without melting. Hypoid gear lubricants and heavy-duty type cutting fluids are examples of extreme boundary lubricants.
5. Clean metal surfaces. This represents the extreme in adverse conditions of sliding contact. Hardness, shear strength, and surface finish are the main characteristics of interest in this type of action.

Real Area of Contact

All finished surfaces are found to have irregularities that are very large in comparison with atomic dimensions (i.e., large compared with 10^{-8} in or 3×10^{-10} m).

As a consequence of these micro irregularities, the real area of contact (A_R) is much less than the apparent area of contact (A). For example, if two carefully ground blocks, each of 1 in^2 cross-sectional area, are placed in contact and loaded with 10 lb, the real area of contact will be less than 10^{-4} in^2 (< 0.1 mm^2), while of course the apparent area (A) is actually 1 in^2 (645 mm^2). When such surfaces first make contact, A_R is zero. As load is applied, the relatively few high points that make contact are plastically deformed and A_R increases. Thus, the real area of contact will be independent of the apparent area of contact or the surface finish but will be determined solely by the applied load and the flow stress or hardness of the protuberances. The area A_R developed must be just sufficient to equal the applied load (P) divided by the hardness (H) of the metal asperities, or

$$P = A_R H \tag{10.1}$$

The characteristic roughness found on most surfaces consists of irregularities with a pitch that is at least an order of magnitude greater than the peak-to-valley distance.

Freshly generated surfaces will be clean but will quickly oxidize or be covered by an adsorbed layer of water vapor or other material depending on the environment and properties of the metal. A freshly generated surface will have a density of electrons and an atom spacing corresponding to the metal in bulk. However, electrons will leave the surface (these are called exoelectrons) as the atom spacing increases to the equilibrium value. The energy associated with the formation of a new surface after equilibrium has been established is called surface energy (T), $[FL/L^2]$. Freshly generated surfaces are extremely active chemically before equilibrium is established.

Beilby (1921) showed that the upper layer of a polished surface is different from the underlying material. His microscopic observations led him to believe that, in polishing, surface metal is caused to move from point to point as though it were molten. The net effect was to smooth the surface by transferring metal from peaks to valleys. Beilby further observed that the resulting surface layer had a glasslike or amorphous structure. The existence of such an amorphous Beilby layer on polished metals has been disputed for many years, electron diffraction data being used successively to prove and disprove the existence of such a layer. More recently, a high-energy laser beam has been used to traverse surfaces following a rastor pattern to produce a surface texture that resembles the Beilby layer. In this case (laser glazing), a very thin layer of metal is melted and then solidifies so rapidly by heat flowing into the cold subsurface that either an amorphous surface is produced or one that has a crystal size so small as to be unresolvable.

Bowden (1945) has presented the most logical arguments in favor of the existence of the Beilby layer. He points out that, in the polishing process, the polishing agent is generally embedded in a relatively soft lap, which is rubbed against the specimen in the presence of some vehicle such as water. Hot spots will develop at the points of contact between the abrasive and the specimen, and local surface temperatures up to the melting point of the metal may be encountered if the polishing speed is sufficiently high. The molten or softened metal will be smeared over the surface and will quickly solidify to form the layer which Beilby observed. Probably the molten surface layer solidifies so rapidly that the crystals produced are extremely small and the material appears amorphous by present methods of study. Bowden states that this hypothesis may be tested by the following procedure: if polishing is due primarily to mechanical abrasion, then the relative hardness of specimen and polisher is the property of importance; but if the action is caused by surface melting, then the relative melting points are of major concern. In a series of simple experiments, it was observed that camphor, which melts at 350 °F (177 °C), readily polishes metals that melt at a lower temperature, such as Woods metal, but has no effect on tin, lead, white metal, or zinc, all of which melt at higher temperatures. That camphor is softer than Woods metal indicates that relative hardness is unimportant. Similarly, zinc oxide, which is comparatively soft, readily polishes quartz, which is harder, because the melting point of zinc oxide is higher than that of quartz. Many other cases support the view that the relative melting point is the important property, rather than hardness, when choosing a polishing agent.

Origins of Friction

The friction of a lightly loaded slider is due to one or a combination of the following causes (ignoring viscous effects):

1. adhesion (fracture of microwelds formed at the tips of contacting asperities)
2. plowing or burnishing (displacement of metal without generation of wear particles)
3. abrasion (microcutting action producing fine chips, i.e., wear particles)
4. transverse displacement (movement of one surface transversely to the other against the applied load due to interference of hard strong asperities)

Rules of Dry Sliding

When two dry clean surfaces slide together under relatively light load, the following rules pertain over a fairly wide range:

1. The coefficient of friction is independent of the applied load.
2. The coefficient of friction is independent of the sliding speed.
3. The coefficient of friction is independent of surface finish.
4. The coefficient of friction is independent of the apparent area of contact (A).
5. The coefficient of friction is independent of the temperature of the sliding surfaces.

The first of these rules is known as Amontons' law (Amontons, 1699). All of these rules fail to hold at extreme values. For example, the coefficient of friction at zero speed (static friction) is normally greater than the dynamic value. Also, the coefficient of friction will normally decrease with speed above that required to cause thermal softening of the less refractory surface. However, for speeds between these two extremes, the coefficient of friction will be approximately independent of speed.

A lightly loaded slider is one for which Amontons' law represents a good approximation (μ independent of P).

Adhesive Friction

For two surfaces in adhesive sliding contact, the friction force (F) will be

$$F = \alpha \tau A_R \tag{10.2}$$

where τ is the shear strength of the weaker of the two sliding materials and α is the fraction of the real area that involves clean adhering asperities. For an unlubricated case, α will approach unity.

For dry surfaces sliding in air, the coefficient of friction will be from Eqs. (10.1) and (10.2):

$$\mu = \frac{F}{P} = \frac{\tau A_R}{H A_R} = \frac{\tau}{H} \tag{10.3}$$

For low friction, one of the surfaces should have low shear strength and high hardness. Since this is a combination not found in nature, most bearing metals are designed to consist of a composite in which a low-shear-strength material is smeared over a harder substrate. The copper–lead bearing (small particles of insoluble lead in copper) is one of many examples of bearing materials based on this principle.

When two metal surfaces are forced together, the high points that make contact will weld by establishing metallic bonds, provided the surfaces are clean. The surfaces need not be heated, for a *pressure weld* may be established at room temperature if sufficient pressure is applied. However, when such a weld is produced between materials of high stiffness (i.e., materials of large Young's modulus, E), the junctions at the tops of the asperities frequently rupture when the load is released. Elastic recovery in such cases causes the junctions to rupture one by one as the load is removed. The larger the A_R/A ratio and the smaller the stiffness of the metals united, the smaller will be the tendency for a pressure weld to rupture when load is released.

The blacksmith normally heats two pieces of steel to be united in order to decrease E and increase A_R/A for the limited force that can be applied. Similarly, it is possible to produce a pressure weld between clean indium and silver surfaces at room temperature with very light pressure applied, due to the softness and low E of indium. However, such a weld cannot be formed between steel and silver due to the relatively low A_R/A ratio and high values of E involved.

The importance of a large value of A_R/A is further illustrated by the relative ease with which a fine, freshly drawn glass filament may be made to adhere to a similar filament, compared with larger more rigid glass rods. The greater conformability of thin specimens is also demonstrated by the relative ease of welding freshly cut sheets of mica of thick and thin sections. A large real area of contact may be obtained with little applied pressure by previously depositing films in the liquid state on the surfaces to be joined. When the adhesive is transformed into a solid film by cooling, by evaporation of a solvent, or by polymerization or other chemical change, a strong joint may be obtained.

In addition to the magnitude of the load, the cleanness of the surfaces is also important in pressure welding. If an oxide or other film is present, it may be broken through only with difficulty when a purely normal load is applied between the surfaces. If, however, there is some tangential motion between two contaminated mating surfaces, it is easier to penetrate the film and establish a weld. A brittle oxide or other surface film is more easily penetrated and the blacksmith frequently uses a flux to react with oxide films on surfaces to be joined to render them more brittle and hence more easily pierced.

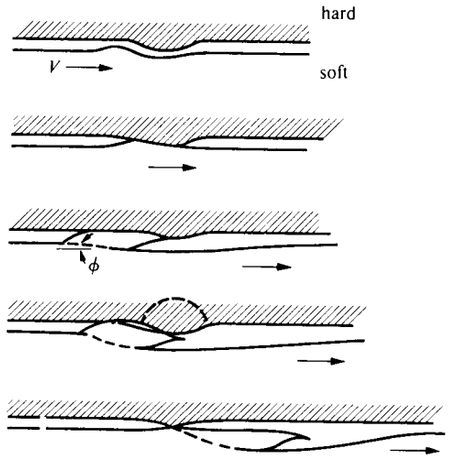

Fig. 10.1 Mechanism of prow formation.

Other Sources of Friction

Cocks (1962, 1964, 1965) has studied the detailed mechanism involved when one dry surface slides over another. Asperities do not simply slide over each other, but what Cocks calls "prows" are produced. These are wedges of plastic metal that tend to force the surfaces apart. By using a flexible system that enabled normal separation of the surfaces by as much as 0.010 in (0.25 mm), large wedges [0.012 in by 0.032 in (0.3 mm by 0.8 mm) in direction of motion] were produced with copper sliding on copper. Figure 10.1 shows the mechanism of prow formation observed when a moving soft asperity encounters a harder one. At (a) the two asperities are about to make contact while (b) shows the asperities shortly after contact. The soft (lower) metal is deformed causing the prow to rise up thus tending to force the surfaces apart. The surfaces deform locally allowing the prow to flow past the hard asperity. With a stiff system, the shear angle (ϕ) will be small and the horizontal prow generating force will be high. The prow generating force will contribute to the friction force and occasionally the strength of the softer material will be exceeded during prow formation giving rise to a wear particle coming from the moving surface. Alternatively, the strength of the harder asperity may be exceeded giving rise to a wear particle coming from the harder (upper) region.

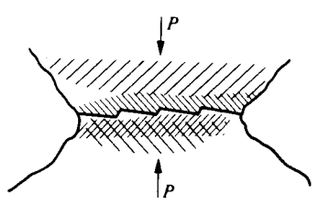

Fig. 10.2 Interface of pair of contacting asperities roughened by plastic deformation. (after Feng, 1952)

Feng (1952) has suggested that the tips of asperities will interpenetrate (Fig. 10.2) due to the inhomogeneous nature of strain associated with the weak points present in all real materials. Subsequent motion will give rise to a friction component of force associated with

1. the transverse displacement of one roughened surface over the other (in the case of hard strong shear plane ends)
2. the shearing-off of the interfering shear plane ends
3. plastic flow of the shear plane ends (burnishing action)

The friction component of force associated with Fig. 10.2 may be due to any combination of the above causes depending upon ductility.

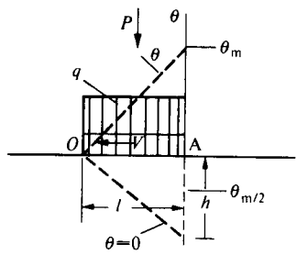

Fig. 10.3 Moving heat source corresponding to a friction slider.

Surface Temperature

When surfaces slide one relative to the other under load, the energy dissipated per unit time is the product of the friction force (F) and sliding speed (V) ($U = FV = \mu PV$). All of this energy is converted into heat. The following approximate analysis is useful in indicating the variables of importance relative to the mean or maximum temperature at the interface for a high speed slider.

Figure 10.3 shows a moving heat source traversing a semi-infinite body subject to the following assumptions:

1. Dispersion of thermal energy over contact area is uniform (q = thermal flux density = thermal units per unit area per unit time).
2. Slider is a perfect insulator—all thermal energy goes to extensive member which has thermal conductivity (k) and volume specific heat (ρC).
3. Slider is extensive perpendicular to paper in Fig. 10.3 (two-dimensional heat flow).
4. Temperature varies linearly from leading edge (O) to trailing edge (θ_m) of slider.
5. Depth of penetration of thermal energy varies linearly from leading edge (O) to trailing edge (h).

Equating the two expressions that may be written for total heat flux, Q,

$$Q = \rho C\left(\frac{\theta_m}{2}\right)(bhV) = k(bl)\frac{\theta_m}{h} \tag{10.4}$$

and hence

$$h = \left[\frac{2kl}{\rho CV}\right]^{1/2} = \left[\frac{2lK}{V}\right]^{1/2} \tag{10.5}$$

where $K = k/\rho C$ = diffusivity, b is slider width, and l is slider length. Substituting into Eq. (10.4),

$$Q = \rho C\frac{\theta_m}{2}(bV)\left[\frac{2lK}{V}\right]^{1/2}$$

or

$$\frac{\theta_m}{2} = 0.707\frac{Q}{b[lV(k\rho C)]^{1/2}} \tag{10.6}$$

The more exact Jaeger (1942) solution leads to the same result except that the coefficient (0.707) is 0.754. However, this agreement is purely fortuitous. What is significant, however, is that the somewhat overly simplified analysis leads to the same functional relationships for ($\theta_m/2$) as the more exact Jaeger approach. Therefore, the coefficient in Eq. (10.6) should be omitted and the mean surface temperature ($\theta_m/2$) merely considered to be proportional to the quantity

$$\left(\frac{Q}{b[lV(k\rho C)]^{1/2}}\right)$$

For a friction slider, q will be constant along the slider if μ is constant and

$$Q = \frac{\mu PV}{J} \tag{10.7}$$

where μ is the mean coefficient of friction, P is the normal load, and J is the mechanical equivalent of heat.

From Eqs. (10.6) and (10.7)

$$\bar{\theta} = \frac{\theta_m}{2} \sim \frac{\mu}{J}\left(\frac{P}{bl}\right)\sqrt{\left(\frac{Vl}{k\rho C}\right)} \tag{10.8}$$

For a high-speed slider, practically all of the thermal energy will be convected away by the extensive member (the slider is a perfect insulator in effect), and Eq. (10.8) will represent a good approximation. This equation states that the mean interface temperature ($\bar{\theta}$) varies

1. directly with the specific friction energy ($\mu P/bl$)
2. directly as $V^{1/2}$
3. directly as $l^{1/2}$
4. inversely as $(k\rho C)^{1/2}$

It is of interest to note that the product ($k\rho C$) of the extensive member is the only thermal property of importance and that the mean and maximum temperatures increase with the length of the slider provided the specific friction energy is constant along the slider.

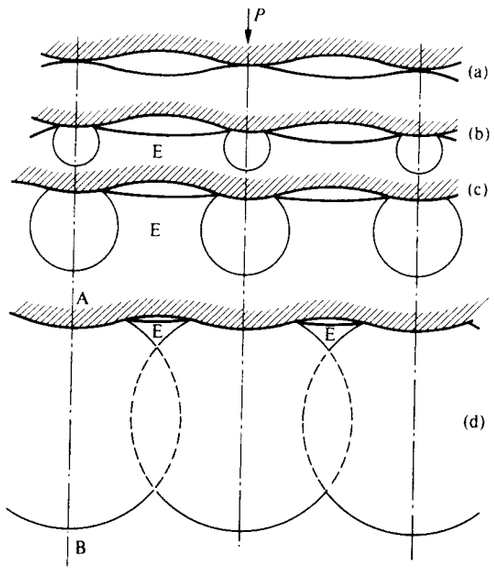

Fig. 10.4 Plane slider under progressively increasing load (P). Upper cross-hatched surface is hard; lower surface is soft. Region E is elastic. (after Shaw, 1963)

Heavily Loaded Sliders

Moore Effect

As the load on a slider increases, the size of the plastic zone associated with each asperity will increase as indicated in Fig. 10.4. At a critical value of load the plastic zones will join up, and then for further increase in load there will be no further flattening of asperities. Instead, the subsurface will flow plastically. Moore (1948) drew attention to this phenomenon by pressing a hard cylinder into a soft copper surface having small parallel grooves [0.025 mm (0.001 in) apart and having a 100° included angle] machined in the surface. He found that even though the subsurface flowed extensively, the grooves were still substantially present (Fig. 10.5).

For an array of flattened asperities, as shown in Fig. 10.6, the mean normal stress on each of the flat areas will be $3Y$, assuming the areas to be far enough apart so there is no interaction between asperities. The asperities should flatten until the total load on all asperities will be just sufficient to cause the subsurface to flow plastically (i.e., until the mean stress in the subsurface = Y).

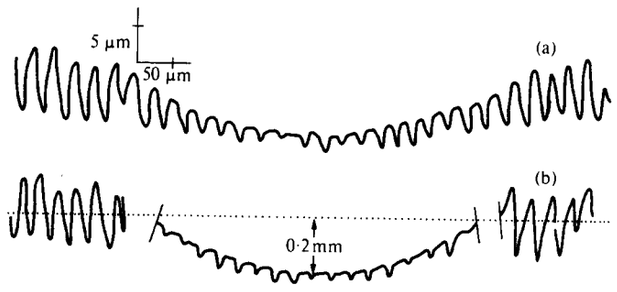

Fig. 10.5 Tallysurf traces of work-hardened copper (H_V 84) having grooves 0.025 mm (0.001 in) apart machined in surface before indentation by 6 mm diameter × 0.18 mm (0.25 × 0.007 in) cylinder. (a) Applied load = 200 kg. (b) Applied load = 2500 kg. (after Moore, 1948)

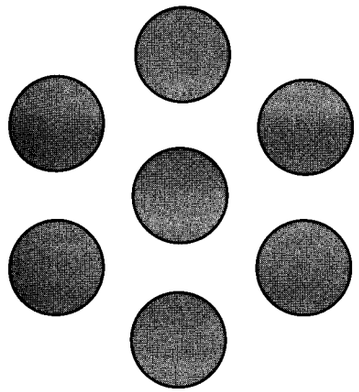

Fig. 10.6 Plan view of asperities flattened by normal stress applied by hard smooth surface.

If asperity interaction is ignored, the real area (A_R) should increase in accordance with Eq. (10.1) until $A_R/A = Y/3Y = \frac{1}{3}$. This represents a relatively crude first approximation since there will be interaction between asperities, and this will cause the limiting A_R/A to be $> \frac{1}{3}$.

Williamson (1968) has performed tests to more exactly identify the transition from a lightly loaded situation to a heavily loaded one. An aluminum specimen with bead-blasted surface was encased in a steel container and loaded by a polished flat piston that closely fitted the steel container. As load was applied, the surface asperities were flattened but did not disappear. Figure 10.7a shows the change in the number of plateaus with load. At first the number increases linearly with load and then remains constant with further increase in load. Figure 10.7b shows the variation in area of contact with load, and this curve is seen to have a knee at about the same load as that where the previous one ceased to rise. Figure 10.7c shows the variation in separation of two surfaces versus load. Again, there is an abrupt change in the slope of this curve at a load of about 900 lb (4009 N) which corresponds to the force required for bulk plastic flow of the specimen. It therefore appears as though the abrupt

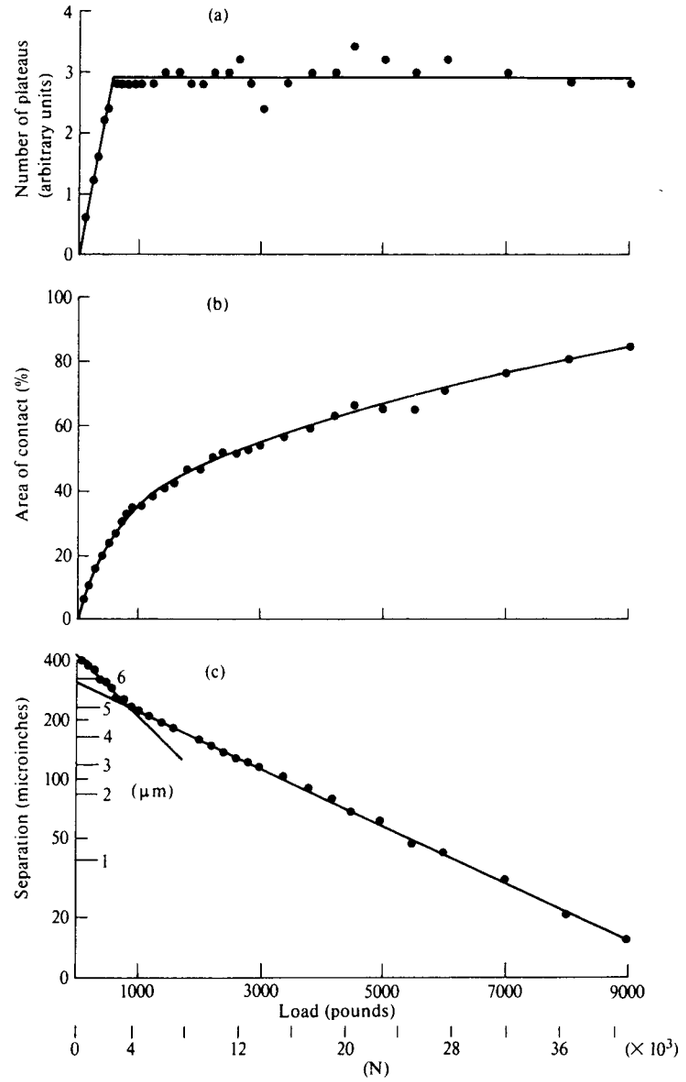

Fig. 10.7 Behavior of contacting surfaces under high normal stress. Bead-blasted aluminum surface encased in a steel container and loaded by a hard-polished steel piston closely fitting the steel container. (after Williamson, 1968)

change in behavior in the curves of Fig. 10.4c to Fig. 10.4d corresponds to a transition from a lightly loaded situation to a heavily loaded one.

From Fig. 10.7b departure from Amontons' law occurs at A_R/A close to the previously predicted value of $\frac{1}{3}$. This suggests that the asperities may in fact act independently of each other as assumed. When the applied load was increased to four times that corresponding to the transition in Fig. 10.7 (4×900 lb $\cong$ 16,000 N), the real area of contact was only 50% of the apparent area.

Junction Growth

Moore (1948) found that when a hard smooth indentor slides across a grooved copper surface, the degree of ridge flattening is greatly increased, the extent of the increase depending upon the coefficient of sliding friction and the direction of the ridges relative to the sliding direction. The friction force will of course help satisfy the flow criterion (either Tresca or von Mises) and the normal stress required for any degree of asperity flattening will be less when a friction force is present. The tendency for the ridges to disappear was greatest when the ridges were oriented normal to the sliding direction since this gave the shortest transport distance associated with the movement of material from peaks to valleys.

Burnishing is a surface-refining operation that requires a high friction force. In wire drawing, surface roughness will be excessive if the friction force is not sufficient to iron out the roughness due to strain inhomogeneity (Fig. 10.2). The challenge is to have sufficient frictional force to provide burnishing without galling. The difference in texture of the front and back of a continuous metal cutting chip is due to removal of shear plane roughness due to burnishing on the tool face but not on the free surface of the chip.

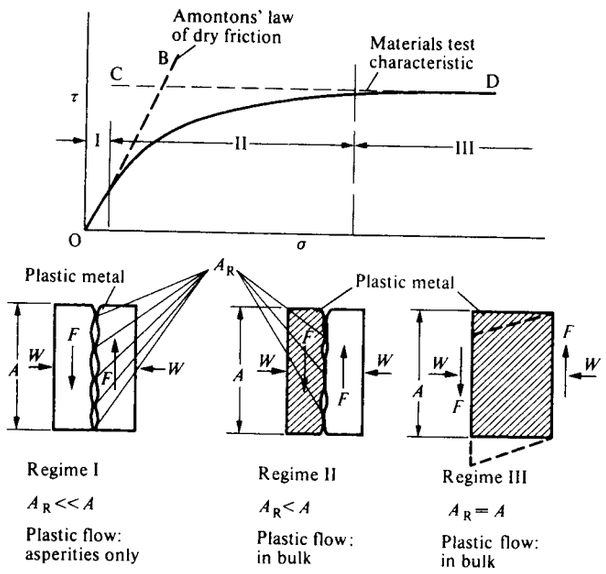

Fig. 10.8 Three regimes of solid friction. (after Shaw, Ber, and Mamin, 1960)

The increase in real area of contact that accompanies sliding (friction) is called junction growth in tribology, and this is what Moore found when a hard smooth indentor was slid across a grooved surface.

Heavily Loaded Slider Friction

Shaw et al. (1960) have presented Fig. 10.8 to illustrate the variation in coefficient of friction with change in normal stress (σ) and hence with (A_R/A). Three regimes are identified. Regime I is that where Amontons' law holds ($\mu = \tau/\sigma =$ constant). Regime III is for an internal shear surface of a material that has not yet developed microcracks ($A_R/A = 1$, and τ is independent of σ). Regime II is the transition region between Regimes I and III. In Regime II, the coefficient of friction ($\mu = \tau/\sigma$) decreases with increase in load. Regime II corresponds to the situation on the tool faces of metal-cutting and -forming tools. Surface sliding is accompanied by subsurface plastic flow in Regime II.

Earlier, Finnie and Shaw (1956) suggested that the ratio of real to apparent area of contact might be approximated as follows:

$$\frac{A_R}{A} = 1 - e^{-BP} \qquad (10.9)$$

where B is a constant for a given material combination, and P is the applied load.

Shaw et al. (1960) have demonstrated the reduction of coefficient of friction with applied load in Regime II using the apparatus shown in Fig. 10.9. A hard steel ball is pressed into a soft steel surface, Brinell fashion, until plastic flow occurs. The torque required to slide the specimen relative to the ball at low velocity is then measured. A small hole is provided at the center to eliminate the singularity that would otherwise exist there. The mean shear stress (τ) and normal stress (σ) may then be estimated for different values of applied load. Figure 10.10 shows representative results where deviation from Amontons' law is clearly indicated as well as the reduction in coefficient of sliding friction with increase in the applied load.

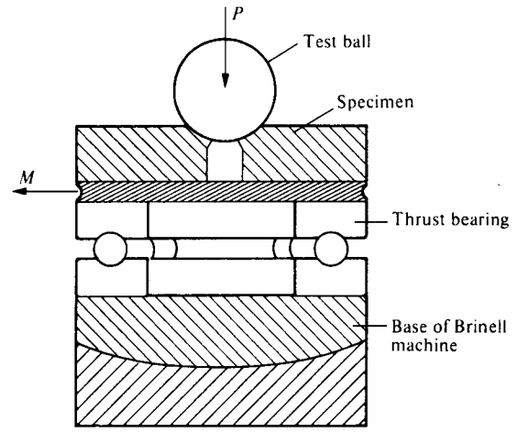

Fig. 10.9 Test apparatus for measuring friction with subsurface plastic flow. (after Shaw, Ber, and Mamin, 1960)

Friction in Metal Cutting

Friction plays an important role on the tool face of a sharp cutting tool and also on the clearance face of a worn tool. However, conditions on the tool face are far different from those for a lightly loaded slider. Amontons' law does not hold over the entire contact area nor do the other rules of dry friction previously discussed for lightly loaded sliders. The complexities of tool-face friction are discussed in a monograph by Bailey (1975).

Stress Distribution on Tool Face

Usui and Takeyama (1960) studied the distribution of shear (τ_C) and normal (σ_C) stress along the tool face of a cutting tool by cutting lead at low speed with a photoelastic tool. Results of this study are shown in Fig. 10.11. The shear stress (τ_C) was found to remain constant over the half of tool–chip contact nearest the cutting edge but to decrease to zero over the other half, reaching

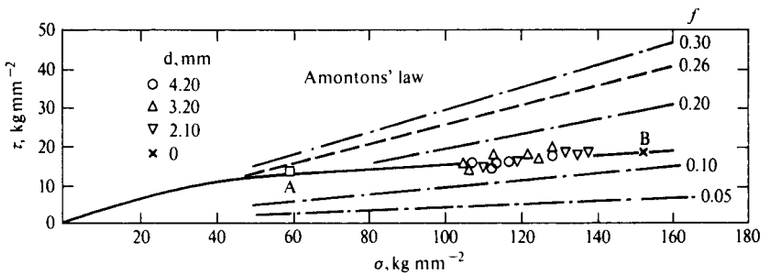

Fig. 10.10 Variation of τ and σ for unlubricated hard steel Brinell ball of $\frac{1}{2}$ in (12.7 mm) diameter tested against mild steel in apparatus of Fig. 10.9. Diameter d is the size of the central hole drilled in the specimen before test. Point A is for subplastic load. (after Shaw et al., 1960)

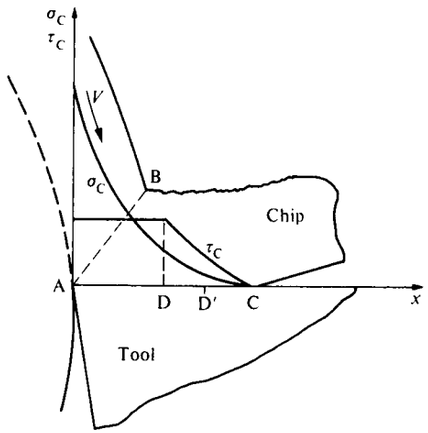

Fig. 10.11 Variation of shear and normal stresses on tool face of tool. (after Usui and Takeyama, 1960)

zero of course at point (C) where the chip leaves contact with the tool. The normal stress (σ_C) was found to increase monotonically from (C) to the cutting edge (A). Zorev (1963) reached similar conclusions by observing that grinding scratches parallel to the cutting edge were transferred to the fully plastic surface of the chip from A to D, but that these markings were replaced by an orthogonal set of scratches running in the direction of chip motion over the second region of contact extending from D to C where sliding actually occurred. Zorev concluded that chip flow was completely within the chip (subsurface) from A to D but occurred at the interface from D to C. Kato and Yamaguchi (1972) used a special tool dynamometer with divided rake face to verify these results. They found stress distributions similar to those of Fig. 10.11 and that the region of constant shear stress decreased relative to total contact length as the rake angle increased.

Figure 10.11 is consistent with the microcrack theory of plastic flow presented in Chapter 9. From A to D, the normal stress (σ_C) is sufficiently high to suppress microcrack formation, the dislocation mechanism pertains, and conditions are similar to those in the Lankford–Cohen experiments. The shear stress (τ_C) will be independent of normal stress (σ_C) over this no-microcrack region (from A to D) and will remain constant at a value consistent with the secondary shear strain pertaining in the chip adjacent to the tool face. Microcracks will be involved in the region of decreasing shear stress (τ_C) extending from D to C. Initially (from D to D′) relatively few microcracks will be involved since the normal stress (σ_C) will be sufficiently high to cause appreciable rewelding. However, as (σ_C) decreases, there will be less and less rewelding relative to fracture, and conditions will approach those for a lightly loaded slider where $A_R/A \ll 1$ and the "microcracks" communicate. The picture of tool-face stresses shown in Fig. 10.11 has been further verified and elaborated recently by other workers (Amini, 1968; Trent, 1977).

In contrast to Fig. 10.11, several studies have revealed sliding at the chip–tool interface near the tool tip but not in the region where the chip leaves contact with the tool (Horne et al., 1977; Doyle et al., 1979; Madhavan et al., 1996). These tests involved transparent single crystal Al_2O_3 (sapphire) tools to cut ductile materials (lead, aluminum, and copper) at very low speed. Under these conditions the chip–tool interface could be directly observed at magnifications as high as 450x, and slip at the tool tip but not at the separation point was clearly evident. The explanation for this paradox appears to be material and speed related.

In the case of lead, the shear strength is so low relative to the bond strength between lead and Al_2O_3 that slip is not prevented even under the relatively high normal stress at the tool tip. At the exit region between chip and tool, the contact stress falls rapidly and A_R/A will be less than one. At low cutting speed, air can penetrate the exit region and react with the chemically active new chip surface to produce lead oxide or lead nitride that has a greater shear strength than the bond strength with Al_2O_3. This apparently accounts for the absence of slip at the exit region when lead is cut at a very low speed. A similar explanation holds for aluminum and copper when cut at very low speed.

Bagchi and Mittal (1988) have performed experiments on steel aluminum and brass using sapphire tools to enable direct observation of the chip–tool interface, but at higher more realistic cutting speeds using a movie camera instead of direct observation. Under steady state conditions two zones were observed corresponding to those of Fig. 10.11. It thus appears that when metals are

cut at practical cutting speeds (above that where a BUE disappears), conditions at the tool–chip interface are well approximated by Fig. 10.11. However, lead which does not produce a BUE is a special case where the sticking and sliding zones are reversed for reasons given above.

It has been suggested by De Chiffre (1977) that only region DC (Fig. 10.11) is influenced by a cutting fluid and that an effective fluid causes a decrease in length DC and hence a decrease in length AC which in turn causes an increase in the shear angle ϕ and a decrease in cutting force. The only change the microcrack theory of Chapter 9 would suggest relative to this concept of cutting fluid action is that the primary action of the cutting fluid extends from D′ to C (Fig. 10.11) where the microcracks communicate like the holes in a sponge. The results of Fig. 9.7 suggest that point D corresponds to the point where $\sigma_C \cong \tau_C/2$.

As Zorev (1963) pointed out, Amontons' law of sliding friction (coefficient of friction is independent of normal stress) should not be expected to hold in the region extending from A to D but only from D to C in Fig. 10.11. There will obviously be a transition region (D to D′), and it would now appear to be more accurate to suggest that Amontons' law will hold only from D′ to C.

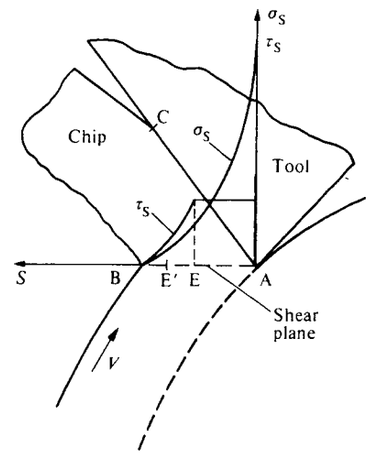

Fig. 10.12 Proposed variation of shear and normal stress across shear plane. (after Shaw, 1980)

It has been suggested by Shaw (1980) that the situation on the shear plane is similar to that on the tool face. Figure 10.12 shows the proposed variation in shear (τ_S) and normal (σ_S) stress on the shear plane with distance across the shear plane. In region AE (nearest the cutting edge), τ_S will be independent of normal stress on the shear plane (σ_S), while in region E′B (nearest the free surface) τ_S/σ_S will be approximately constant corresponding to Amontons' law for a friction slider. These two regions should be connected by a transition region (EE′ in Fig. 10.12) where the density of microcracks is increasing to the point of intercommunication. Figure 10.12 explains why the microcracks mechanism of plastic flow of Chapter 9 involving the rewelding of microcracks should be expected to pertain over part of the shear plane in metal cutting even though the *mean* normal stress on the shear plane will generally be $\geq \bar{\tau}_S$.

Variation of Coefficient of Tool–Face Friction with Rake Angle

One of the paradoxes associated with metal cutting involves the variation of tool–face friction coefficient (μ) with rake angle (α). Table 10.1 presents typical orthogonal cutting data for copper and steel cut at low speed with high speed steel (HSS) tools in air. The stresses were calculated from measured forces and contact areas on the tool face. These stresses (τ_C and σ_C) are based on the apparent area and are assumed to be uniformly distributed. It is clearly evident that the coefficient of cutting friction increases markedly with increase in rake angle. This is just the opposite behavior one would expect from experience with lightly loaded sliders that perform in accordance with Amontons' rule. However, it is what should be expected from heavily loaded slider experience where the coefficient of friction ($\mu = \tau_C/\sigma_C$) is found to decrease with increase in normal stress as a consequence of an increase in A_R/A. It may therefore be concluded that the paradox is in part explained by the fact that conditions at the tool face are largely those of a heavily loaded slider.

An additional reason for the tool–face friction paradox appears to lie in the fact that the friction process in cutting interacts strongly with the shear process. As a first crude approximation, we may characterize the shear process in terms of the Lee–Shaffer (1951) model which appears to be one of

TABLE 10.1 Representative Low-Speed Cutting Data

Work Material	Rake Angle α (deg)	Average Stresses at Tool–Chip Interface (p.s.i.†) Shear Stress (p.s.i.) τ_C	Normal Stress (p.s.i.) σ_C	Mean Friction Coefficient $\mu = \tau_C/\sigma_C$
Electrolytic tough pitch copper; cutting speed (V), 0.3 f.p.m. (0.0016 m s^{-1}); depth of cut (t), 0.002 in (0.05 mm)	30	35,600	43,300	0.82
	45	34,700	30,000	1.15
	60	36,700	16,000	2.30
SAE B1112 steel; cutting speed (V), 0.04 f.p.m. (0.0002 m s^{-1}) depth of cut (t), 0.003 in (0.076 mm)	16	46,000	70,000	0.66
	30	49,300	57,000	0.86
	45	51,700	43,200	1.20

† 1 p.s.i. = 6905 N m^{-2}.

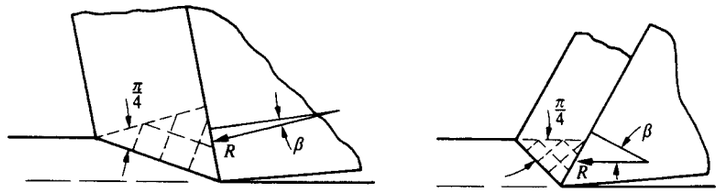

Fig. 10.13 Variation in magnitude and direction of resultant cutting force with rake angle.

the least objectionable simple models yet proposed. Figure 10.13 shows the slip line fields for sharp high- and low-rake-angle tools cutting the same materials. Assuming the shear plane to be a plane of maximum shear stress and the resultant cutting force (R) to be displaced 45° from the shear plane in accordance with the Lee–Shaffer solution, angle β ($\beta = \tan^{-1}\mu$) will be smaller for a negative rake angle.

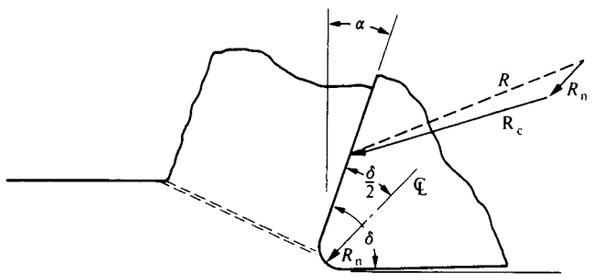

Fig. 10.14 Influence of tool tip radius on cutting forces. [R_n = Indenting force due to tool radius. R_c = Resultant cutting force on remainder of tool face.] (after Masuko, 1953)

Indentation Force at Tool Tip

Masuko (1953) suggested that a sharp cutting tool will deform elastically to give a radius at the tip of even a sharp cutting tool. Figure 10.14 shows a cutting tool with the assumed radius at the tip. Masuko assumed that in addition to the chip forming force (R_c) on the tool face, there would be an indentation force at the tool tip (R_n in Fig. 10.14). He assumed that the indentation force R_n bisects the included angle of the tool (δ). The components of indentation force R_n were substracted from the measured force components F_P and F_Q and the resulting values used to compute stresses and strains as outlined in Chapter 3.

The concept of an indenting component of force was probably suggested to Masuko by the fact that when measured values of F_P and F_Q are plotted against undeformed chip thickness (t), straight lines with an intercept at $t = 0$ are obtained as shown diagrammatically in Fig. 10.15. The cutting (R_{nP}) and feed (R_{nQ}) components of indentation force R_n were assumed to correspond to the intercepts of the F_P and F_Q versus t curves in Fig. 10.15.

The actual values of R_{nP} and R_{nQ} were obtained by an iterative approximate elastic analysis. When the above procedure was applied to data for a duralumin specimen cut dry using HSS tools having rake angles ranging from 0 to 44°, the coefficient of friction for cutting on the tool face was found to be constant relative to α and t. At the same time when the shear stress on the shear plane (τ) was compared with extrapolated values of τ versus γ for torsion tests on the same material, no size effect was found. However, in extrapolating the torsion data to the larger strains pertaining in cutting, Eq. (5.8) was used instead of Eq. (9.11). From these results, Masuko concluded that there is no size effect in cutting and that the unusually high values of shear stress on the shear plane in cutting are due to strain hardening alone.

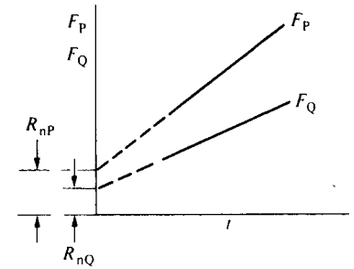

Fig. 10.15 Variation of power (F_P) and feed (F_Q) components of cutting force with undeformed chip thickness (t). R_{Pn} and R_{Qn} are the horizontal (power and vertical components of R_n in Fig. 10.14.

Results practically identical to those of Masuko have been reported by Albrecht (1960, 1961, 1963).

While the proposal of Masuko is logical, it does not appear to hold up when subjected to critical experiment. Finnie (1963) has performed orthogonal cutting tests on a perfectly sharp tool and one of very small bluntness. Figure 10.16 gives his results. These curves show that whereas the force versus feed curves pass through the origin for the sharp tool, the blunt tool has intercepts. From these results, extrapolation of force versus undeformed chip thickness (t) data to $t = 0$ is seen to be a questionable procedure for a sharp tool. The nonlinearity of the force versus undeformed chip thickness curves for the sharp tool is direct evidence of a size effect (increase in flow stress of material cut with decrease of t). Finnie's results indicate that the height of the rounded nose of a blunt tool must exceed about 20% of the undeformed chip thickness (t) before its influence becomes noticeable.

Finnie (1963) also suggests that the general absence of a deformed layer on surfaces produced by sharp tools argues against the general importance of an indentation or plowing in metal cutting. However, the indentation or ploughing effect should be expected to be important in grinding (very small t and large negative rake angle) or for tools of appreciable dullness.

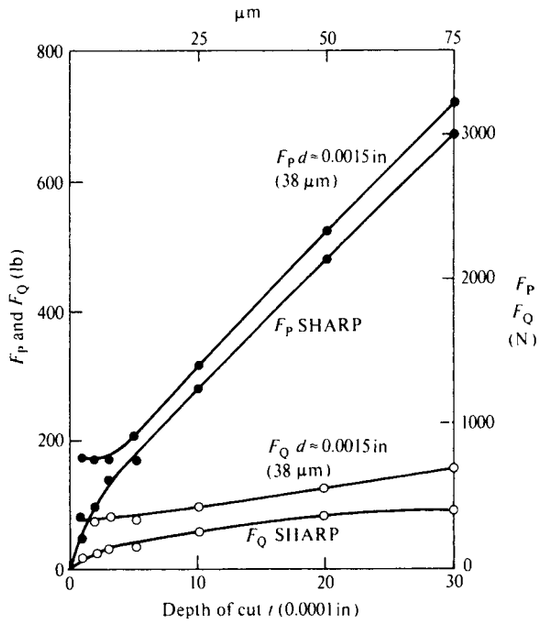

Fig. 10.16 Variation of cutting force components in velocity (F_P) and feed (F_Q) directions with undeformed chip thickness (t) for sharp and dull tools. Dimension d is extent of tool bluntness measured in feed direction. (after Finnie, 1963)

Stevenson and Stephenson (1995) have performed cutting tests on pure zinc to further explore the possibility of a plowing effect existing at the tip of a sharp tool to account for the extrapolated intercepts at $t = 0$ shown in Fig. 10.15. Compression values of stress and strain for cylindrical specimens of the same material (zinc) were extrapolated to obtain corresponding metal cutting results. The von Mises criterion was used in making adjustments for differences in temperature, strain, and strain rate. Using the same analytical approach it was found that when the undeformed chip thickness values (t) for cutting with a sharp tool were extrapolated to zero, any plowing effect was found to be negligable. It was inferred that the following results would hold for other metals as well as for zinc:

(a) negligable plowing for a sharp tool

(b) ability to extrapolate compression test data to cutting conditions using the von Mises criterion

However, while item a is in agreement with the results of Finnie (Fig. 10.16), item b which holds for pure zinc does not agree with results for steel as the experiments of Merchant in Chapter 8 clearly indicate. The probable reason for this is discussed in Chapter 9. This involves the appearance and transport of microcracks as well as dislocations when metals are subjected to very high strains (1.5 or higher) as in the steady state chip formation of steel.

Multiplicity of Mechanisms

Metal cutting is an extremely complex process that cannot be described by a single simple mechanism. While a single mechanism may be predominant over a limited range of operating conditions, experience teaches that no single mechanism holds in general. This accounts for the extremely wide range of views that have appeared in the literature to explain cutting results, most of which are supported by sound experimental data. In most cases, the relatively simple mechanism suggested by an author to explain his or her results fails to hold when applied to substantially different operating conditions. This condition has led Hill (1954) to suggest that no unique solution exists as already discussed in Chapter 8.

References

Albrecht, P. (1960). *J. Engng. Ind.* **82**, 348.
Albrecht, P. (1961). *J. Engng. Ind.* **83**, 557.
Albrecht, P. (1963). *International Research in Production Engineering*. ASME, New York, p. 32.
Amini, E. (1968). *J. Strain Anal.* **3**, 206.
Amontons, G. (1699). *Historie de L'Academie Royale des Sciences avec les Memories de Mathematique et de Physique*, p. 206.
Bagchi, A., and Mittal, R. O. (1988). *Proc. of Manufracturing International, Atlanta, Ga.*
Bailey, S. A. (1975). *Wear* **31**, 243.
Beilby, G. (1921). *Aggregation and Flow of Solids*. Macmillan, London.
Bowden, F. P. (1945). *Proc. R. Soc. N.S.W.* **78**, 187.
Bowden, F. P., and Tabor, D. (1950). *The Friction and Lubrication of Solids*, Vol. I. Clarendon Press, Oxford.
Bowden, F. P., and Tabor, D. (1964). *The Friction and Lubrication of Solids*, Vol. II. Clarendon Press, Oxford.
Cocks, M. (1962). *J. Appl. Phy.* **33**, 2152.
Cocks, M. (1964). *J. Appl. Phys.* **35**, 1807.
Cocks, M. (1965). *Int. J. Wear* **8**, 85.
De Chiffre, L. (1977). *Int. J. Mach. Tool Des. Res.*, 225.
Doyle, E. D., Horne, J. G., and Tabor, D. (1979). *Proc. Roy. Soc. of London* **A-366**, 173–187.

Feng, I. M. (1952). *J. Appl. Phys.* **22**, 1011.
Finnie, I. (1963). In *International Research in Production Engineering*. ASME, New York, p. 76.
Finnie, I., and Shaw, M. C. (1956). *J. Engng. Ind.* **78**, 1649.
Hill, R. (1954). *The Mathematical Theory of Plasticity*. Clarendon Press, Oxford. (Reissued 1983.)
Horne, J. G., Doyle, E. D., and Tabor, D. (1977). Proc. of 5th N.A. Metal Working Research Conf. of 5ME, pp. 237–241.
Jaeger, J. C. (1942). *Proc. R. Soc. N.S.W.* **76**, 203.
Kato, H., and Yamaguchi, K. (1972). *Proc. ASME* **94**, 603.
Madhavan, V., Chandrasekar, S., and Farris, T. N. (2002). *ASME J. of Tribology* **124**, 617–626.
Masuko, M. (1953). *Trans. Jap. Soc. Mech. Engrs.* **19**, 32.
Moore, A. J. W. (1948). *Proc. R. Soc.* **A195**, 231.
Shaw, M. C. (1963). *Int. J. Wear* **6**, 140.
Shaw, M. C. (1980). *Int. J. Mech. Sci.* **22**, 673.
Shaw, M. C., Ber, A., and Mamin, P. A. (1960). *J. Engng. Ind.* **82**, 341.
Stevenson, R., and Stephenson, D. A. (1995). *Trans ASME-J. of Eng. Materials and Technology* **117**, 172–178.
Suh, N. P. (1986). *Tribophysics*. Prentice-Hall, Englewood Cliffs, N.J.
Suh, N. P., and Sin, H. C. (1981). *Wear* **49**, 9.
Trent, E. M. (1977). *Metal Cutting*. Butterworths, London.
Usui, E., and Takayama, H. (1960). *J. Engng. Ind.* **B82**, 303.
Williamson, J. B. P. (1968). In *Interdisciplinary Approach to Friction and Wear*. Office of Technology Utilization, Washington, D.C., p. 85.
Zorev, N. N. (1963). In *International Research in Production Engineering*. ASME, New York, p. 42.